

# Insights into the origins and growth of supermassive black holes

Yash Aggarwal

Lamont-Doherty Earth Observatory of Columbia University,  
Emeritus Associate  
Palisades, NY 10965, USA  
E-mail: hagggarwal@hotmail.com

## ABSTRACT

We present a well-tested, theoretically supported empirical relation that helps decipher the origins, growth, and properties of supermassive black holes (SMBHs). Based on theoretical considerations and analysis of mass ( $M_{\text{BH}}$ ) versus age ( $t$ ) distribution of 93 high-redshift ( $>5.6$ ) SMBHs, we get  $M_{\text{BH}} = M_s \exp [14.6(t-100)/t(\text{Myr})]$ , which gives the SMBH's seed mass  $M_s$ , and its derivative gives the instantaneous mass-accretion rate. It yields seeds of  $\sim 20\text{-}420M_{\odot}$  (solar masses) for the recently discovered SMBHs GNz11, CEERS\_1019, and UHZ1, and  $\sim 3 \times 10^4 M_{\odot}$  for the largest ( $1.24 \times 10^{10} M_{\odot}$ ) high- $z$  SMBH. It is applied to 132446 SMBHs at  $z < 2.4$  cataloged by Kozłowski. The resultant seeds are classified based on size and likely formation mechanism:  $\sim 58\%$  are light ( $< 400M_{\odot}$ ) deemed to be Pop III remnants;  $\sim 39\%$  are intermediate ( $400\text{-}3 \times 10^3 M_{\odot}$ ) and  $< 3\%$  heavier seeds ( $3 \times 10^3 M_{\odot}\text{-}3 \times 10^4 M_{\odot}$ ), both of which formed possibly by mergers of Pop III remnants. The DCBH mechanism is not required but not excluded. Furthermore, the results show the following. The mass-accretion rate increases exponentially from the seed's inception ( $z \sim 30$ ), reaches a broad plateau at  $z \sim 8.5\text{-}6$  coincident with the epoch of reionization, and decreases monotonically. Sub-Eddington accretion is the norm, except during the first  $\sim 150$  Myrs, SMBHs experienced super-Eddington accretion, or the radiative efficiency was  $< 0.1$ . The largest seed can potentially grow via luminous accretion to  $(6.6 \pm 2.2) \times 10^{10} M_{\odot}$ , consistent with a theoretical limit of  $\sim 5 \times 10^{10} M_{\odot}$  by King. The Eddington ratio decreases and radiative efficiency increases as  $z$  decreases, consistent with recent findings.

**Key words:** black hole physics –galaxies: fundamental parameters –galaxies: nuclei –quasars: supermassive black holes - stars: black holes.

# 1. INTRODUCTION

It is generally accepted that supermassive black holes (SMBHs) grew from progenitor seeds formed or assembled in the early universe. However, it remains unclear how massive these seeds were. Were they predominantly light or heavy, or somewhere in between? The origins of the black holes (BH) or the mechanisms by which they may have formed are intimately related to seed size. Proposed mechanisms by which seeds may have formed have been extensively reviewed, among others, by Latif and Ferrara (2016) and Volonteri et al. (2022) and can broadly be divided into three categories depending on the size of the seeds. Light seeds with a typical mass of  $\sim 100M_{\odot}$  formed from the collapse of massive metal-free first stars (Madau and Rees, 2001; Johnson and Bromm, 2007) dubbed as Pop III remnants. Formation of heavy seeds  $10^4M_{\odot}$ - $10^6M_{\odot}$  from the collapse of pristine gas clouds in massive dark matter halos (Bromm and Loeb, 2003; Begeleman et al., 2006; Lodato and Natarajan, 2006; Shang et al., 2010) dubbed as DCBHs, or by hierarchical growth of BHs in dense stellar clusters (Davies et al., 2011). And the formation of intermediate-size ( $\sim 10^3M_{\odot}$ ) seeds via runaway collisions of stars in dense stellar clusters (Portegies et al., 2004; Freitag et al., 2006; Mapelli, 2016) or by hierarchical merger of BHs in stellar clusters (Davies et al., 2011; Lupi et al., 2014). Simulations attempting to understand the properties of the seeds formed by such mechanisms, drawbacks, and conditions necessary for their formation have also been extensively reviewed (see Latif and Ferrara, 2016; Volonteri et al., 2022). It is safe to conclude that there is no consensus as to which of the proposed mechanisms may have played a dominant role and presumably cannot be ascertained without knowing the size distribution of the seeds formed.

Furthermore, black hole seeds are thought to have formed at  $z \sim 20$ – $30$  (Barkana & Loeb 2001), and the recent discovery of the AGN GNz11 at  $z=10.6$  (Maiolino et al., 2024) supports such an assumption. The existence of active galactic nuclei (AGN) exceeding  $10^{10}M_{\odot}$  (solar masses) less than a billion years old (e.g., Wu et al., 2015) has, however, defied comprehension as to how these seeds grew so massive in such short times. This dilemma is best illustrated by the following case studies of three recently discovered SMBHs at  $z \geq 8.7$ . Larson et al. (2023) concluded that CEERS\_1019 at  $z \sim 8.7$  and  $M_{\text{BH}} \sim 9 \times 10^6 M_{\odot}$  requires super-Eddington accretion from stellar-sized seeds or Eddington limited from massive BHs seeds. Schneider et al. (2023) and Maiolino et al. (2024) concluded that GNz11 at  $z=10.6$  and  $M_{\text{BH}} \sim 1.5 \times 10^6 M_{\odot}$  is accreting respectively at Eddington ratio  $\lambda$  of  $\sim 2.5$  and  $5.5$ . In contrast, using simulations, Bhatt et al. (2024) found that the probability of observing a BH at  $z \sim 10$ – $11$  accreting with  $\lambda \sim 5.5$  in the volume surveyed by JWST is  $< 0.2\%$ . And for the third AGN UHZ1 at  $z \sim 10.1$  with an estimated  $M_{\text{BH}} \sim 4 \times 10^7 M_{\odot}$ , Natarajan et al. (2024) concluded that it grew from a heavy seed ( $\sim 10^4 M_{\odot}$ ) formed at  $z \sim 14$  that was probably a DCBH. Again, it is safe to conclude that there is no consensus or clear understanding of how SMBHs, starting from progenitor seeds orders of

magnitude smaller, grew to their observed sizes in several hundred million to less than a billion years.

While studies of individual AGNs provide valuable insights into the properties of that BH and may support a particular theory of the formation or growth of BH seeds, they cannot rule out other theories or channels of seed formation (Volenteri et al., 2022); nor do such studies provide measures of the growth rates of SMBHs. Presumably, solving the dual interrelated enigma of the origins and growth of SMBHs requires insights and constraints derived from large sets of observational data. The JWST may provide such data in years to come. Meanwhile, a large corpus of publicly available data, comprising known properties (redshift, mass  $M_{\text{BH}}$ , Eddington ratio  $\lambda$ ) of over a hundred thousand AGNs at various redshifts, remains largely unexploited. More precisely, this corpus consists of about 93 high- $z$  AGNs at  $z > 5.6$  whose masses are well constrained and range over four orders of magnitude and  $\sim 560$  Myr in age, and 132,446 lower- $z$  AGNs at  $z < 2.4$  and  $M_{\text{BH}} \geq 10^7 M_{\odot}$  determined using MgII lines by Kowłowski (2017). Fragione and Pacucci (2023) have attempted to constrain the distribution of BH seeds using a catalog of 113 high redshift ( $z > 6$ ) AGNs compiled by Fan et al. (2023). Applying Bayesian analysis to these AGNs, they concluded that light and heavy seeds are required, whose distribution can be modeled by combining a power law and a lognormal function. Furthermore, they obtained mean values for the Eddington ratio, duty cycle, and radiative efficiency of the high- $z$  AGNs. Here, prompted by new insights garnered from a deconstruction of a commonly used theoretical formula for the growth of a black hole (BH), we analyze the mass versus age distribution of the 93 high redshift AGNs and derive an empirical relation expressing a BH's mass  $M_{\text{BH}}$  as a function of its age  $t$  or redshift  $z$  and the mass  $M_s$  of its seed, from which the seed mass  $M_s$  can be ascertained knowing the BH's mass  $M_{\text{BH}}$  and redshift. The derivative of this primary relation gives a BH's accretion rate at any instant of its active life. Furthermore, using a BH's instantaneous accretion rate thus derived, its radiative efficiency can be obtained from its bolometric luminosity. Together, these relations comprise a set of powerful tools to decipher the origins, growth, and properties of SMBHs.

We begin by providing the theoretical basis of the primary relation and then derive the primary empirical relation using observational data. It is first applied to the 93 high- $z$  BHs. The resulting distributions of seed size versus BH mass and BH age are analyzed, and conclusions are drawn regarding the range of seed sizes necessary to account for the masses of the high- $z$  SMBHs observed thus far. In particular, the seed mass required to account for the mass of each of three recently discovered ultra-high  $z$  AGNs, namely GNz11, CEERS-19, and UHZ1, is determined. The primary relation is then applied to the 132,446 AGNs at  $z < 2.4$  to test its universal applicability and the validity of the conclusions drawn from its application to the high- $z$  AGNs. More importantly, the resulting mass distribution of the 132,446 seeds is analyzed and compared to simulations of mass functions of the first massive stars by Hirano et al. (2014) and intermediate-size BHs formed via runaway collisions in nuclear star clusters by Devecchi et al.

(2012) and gas-induced hierarchical growth of BHs by Lupi et al. (2014). Based on this comparison, the population of 132,446 seeds is classified into light, intermediate, and heavier, with corresponding mechanisms likely responsible for their formation. After that, the derivative of the primary relation is used to garner insights into a BH's accretion rate, the Eddington ratio, and the radiative efficiency as functions of redshift and find the role if any super-Eddington accretion plays in the growth of SMBHs. We end with a summary of the principal conclusions.

## 2. THEORETICAL BASIS

Conventionally, a BH's exponential growth is defined by Eq. 1, where  $M_{\text{BH}}$  is the black hole mass,  $t$  its age (Myr),  $M_s$  its seed's mass,  $t_s$  the inception time, 45 Myr the Salpeter time scale ( $t_{\text{Sal}}$ ) for a BH accreting at the Eddington limit, and  $\Upsilon$  a non-dimensional parameter defined in Eq.2 and dubbed the "growth efficiency factor" by Zybovas and King (2022).

$$M_{\text{BH}}(t) = M_s \exp [\Upsilon(t - t_s) / 45(\text{Myr})] \quad (1)$$

$$\Upsilon = [0.11 \delta \lambda (1 - \epsilon) / \epsilon] \quad (2)$$

In Eq.2,  $\lambda$  is the Eddington ratio,  $\epsilon$  the radiative efficiency, and  $\delta$  the duty cycle, all averaged over a BH's active life span ( $t - t_s$ ). Note that for  $\delta = 1$ ,  $\epsilon = 0.1$ , and  $\lambda = 1$ ,  $\Upsilon = 1$ , and  $t_{\text{Sal}} = 45 \text{ Myr}$  and Eq.1 reduces to the conventional Salpeter relation for a BH accreting at the Eddington limit. By definition,  $\lambda = L_{\text{bol}} / L_{\text{EDD}}$ , and the bolometric luminosity  $L_{\text{bol}} \propto (\dot{M} \epsilon / (1 - \epsilon))$  where  $\dot{M}$  is the accretion rate, and the Eddington luminosity  $L_{\text{EDD}} \propto M_{\text{BH}}$ . Hence,  $\Upsilon \propto \delta(\dot{M} / M_{\text{BH}})$  or the accretion rate per unit BH mass. Ostensibly, the accretion rate or  $\Upsilon$  cannot be a constant because a BH of say  $10^{10} M_{\odot}$  at say  $t = 10^9$  years would grow untenably by  $\sim 100$  orders of magnitude by  $t = 10^{10}$  years. On the contrary, evidence shows that  $\delta$  decreases as  $z$  decreases (Shankar et al., 2010), and more recently Aggarwal (2024) has demonstrated that  $\lambda$  decreases as  $z$  decreases, but the radiative efficiency  $\epsilon$  increases as  $z$  decreases, and hence  $(1 - \epsilon) / \epsilon$  decreases as BH ages. Therefore,  $\Upsilon$  or the accretion rate per unit BH mass must be an inverse function of a BH's age  $t$ , and its value averaged over the lifespan would invariably be greater than its value at any instant in the life of a BH. And since  $\Upsilon$  is nondimensional, we can simply define  $\Upsilon = \beta 45 / t$ , where  $\beta$  is a nondimensional proportionality constant and  $t$  in Myr. and 45 Myr is the standard e-folding time. Thus, Eq.1 reduces to Eq.3, where  $M_{\text{BH}}$  is a function of its known age  $t$  and three free parameters:  $M_s$ ,  $\beta$ , and  $t_s$ .

$$M_{\text{BH}}(t) = M_s \exp [\beta (t - t_s) / t] \quad (3)$$

The seed mass  $M_s$  of a BH can be determined using Eq.3 if the values of  $\beta$  and  $t_s$  were known. To obtain the values of the constants  $\beta$  and  $t_s$  in Eq.3, we need three or more BHs of different ages but similar, albeit unknown, seed masses. In the next sections, we determine the optimum value of  $\beta$  and seek constraints on inception time  $t_s$  using publicly available data for SMBHs younger than a billion years.

### 3. OBSERVATIONAL DATABASE

We searched the literature for SMBHs younger than a billion years ( $z > 5.65$ ) whose masses are reliably known. Table A1 (Appendix) lists 59 SMBHs discovered until the end of 2022 with references for data sources. The average reported  $1\sigma$  uncertainty in the  $M_{\text{BH}}$  of the 59 BHs is  $\sim 0.11$  dex. In addition, Shen et al. (2019) list 50 SMBHs within a narrow  $z$  range straddling  $z=6$ , of which the  $M_{\text{BH}}$  of 12 are not well constrained, and 6 are duplicates of those in Table A1. The remaining 32 BHs extracted from Table 3 in Shen et al. (2019) are identified in the Appendix. This compilation of 91 BHs is comparable to that of Fan et al. (2023) for 113 BHs at  $z > 5.3$ , except that we indicate the uncertainty in  $M_{\text{BH}}$  of each BH and have excluded from the list those BHs whose  $M_{\text{BH}}$  are poorly constrained. In addition, there are two more recently discovered BHs at  $z > 8.6$ . These are GNz11 at  $z=10.6$  with  $M_{\text{BH}} \sim 1.5 \times 10^6 M_\odot$  and CEERS\_101911 at  $z \sim 8.7$  with  $M_{\text{BH}} \sim 9 \times 10^6 M_\odot$  for a total of 93. The UHZ1 AGN is omitted because its mass is estimated assuming  $\lambda=1$  (Natarajan et al., 2024) and hence uncertain. At lower redshifts, Kozłowski (2017) lists  $\sim 280,000$  AGN at  $z < 2.4$ , almost all of which have  $M_{\text{BH}} \geq 10^7 M_\odot$ . Of these 280,000 AGN,  $\sim 132,446$  have  $M_{\text{BH}}$  determined using the more reliable MgII lines and Eddington ratios based on a weighted average of bolometric luminosities derived using two or more AGN luminosities. The high- $z$  sample of 93 AGN appears to be skewed in favor of the larger BHs since  $\sim 75\%$  have  $M_{\text{BH}} \geq 10^9 M_\odot$ ; whereas the lower- $z$  sample appears not to be because it has  $\sim 63\%$  in the  $10^8$ - $10^9 M_\odot$  range,  $\sim 27\% \geq 10^9 M_\odot$ , and the rest  $\sim 10\% < 10^8 M_\odot$ . We note that there are probably a few hundred SMBHs at intermediate redshifts of  $2.5 < z < 5.5$  that we did not compile because their inclusion would not alter the results of this study. Note that  $z$  is converted into  $t$  using the Hubble constant ( $H_\odot = 67.4$  km/s/Mpc) and matter density parameter ( $\Omega_m = 0.315$ ) from the Planck group (2020). An SMBH is defined as  $\geq 10^6 M_\odot$ . Throughout this paper,  $M_{\text{BH}}$  and  $M_s$  are in solar masses ( $M_\odot$ ) and age  $t$  in Myr.

### 4. EMPIRICAL RELATIONS

Figure 1 shows the mass  $M_{\text{BH}}$  versus age  $t$  distribution of 91 of the 93 SMBHs with density contours. The two recently discovered at  $t < 600$  Myr fall outside the bounds of Fig.1. Depending on their mass, the BHs in Fig.1 are denoted by three different symbols. Those in blue squares have similar masses within a factor of  $\sim 2$  of  $2.5 \times 10^9 M_\odot$  but different ages covering the entire age spectrum in Fig.1; those in red triangles nominally have  $M_{\text{BH}} > 5 \times 10^9 M_\odot$ , and those in red circles

have  $M_{\text{BH}} < 10^9 M_{\odot}$ . First, we seek to constrain the value of  $\beta$  and understand to what extent  $M_{\text{BH}}$  depends on age  $t$ . For this purpose, we will tentatively assume that the seed inception time  $t_s=100\text{Myr}$  in Eq.3. Equation 3 indicates that  $M_{\text{BH}}$  is directly proportional to seed mass  $M_s$  and increases with age  $t$ . The most massive BHs are the most likely candidates for the heaviest seeds. If so, Eq.3 requires  $\beta \leq 15.85$  for  $M_s \geq 10^4 M_{\odot}$  for the largest high- $z$  BH (#31, Table A1). As for the dependence of  $M_{\text{BH}}$  on  $t$ , the ages of the 91 BHs range from 676-1000Myr and Eq.3 indicates that a BH's  $M_{\text{BH}}$  increases by only a factor of  $\sim 2$  from  $t=676\text{Myr}$  to  $t=1000\text{Myr}$ . for any likely value of  $\beta \leq 15.85$ , compared to the orders of magnitude differences in the  $M_{\text{BH}}$  of the BHs in Fig.1. Hence, within this age range, a BH's  $M_{\text{BH}}$  depends primarily on its seed mass  $M_s$  and relatively little of a BH's age  $t$ .

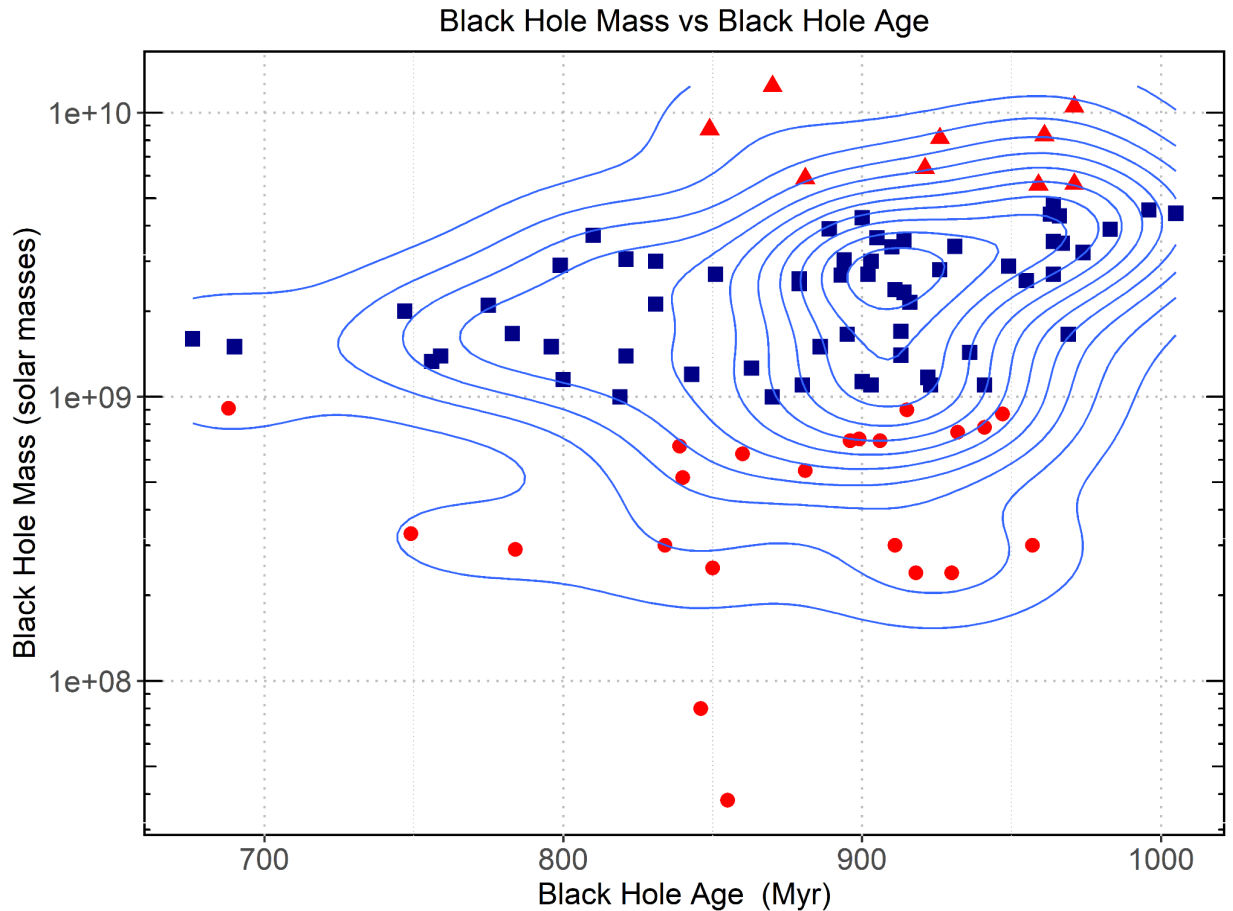


Fig.1 Mass  $M_{\text{BH}}$  versus age  $t$  for 91 SMBHs listed in the Appendix. Density contours are shown. The average reported  $1\sigma$  uncertainty in  $M_{\text{BH}}$  is  $\sim 0.11\text{dex}$ . The 60 BHs denoted by blue squares share a common feature: their masses are within a factor of  $\sim 2$  of  $2.5 \times 10^9 M_{\odot}$ , but their ages span  $\sim 325$  Myr of cosmic time. Those in red triangles nominally have  $M_{\text{BH}} > 5 \times 10^9 M_{\odot}$ , and those in red circles have  $M_{\text{BH}} < 10^9 M_{\odot}$ .

Figure 1 reveals that  $\sim 60$  BHs identified by blue squares have similar masses within a factor of 2 of  $2.5 \times 10^9 M_{\odot}$  but different ages spanning  $\sim 325$  Myr of cosmic time. The inescapable conclusion is that these 60 BHs had similar-sized seeds. Hence, for each of the 60 BHs, we can write Eq.3 with one variable ( $t$ ) and three free parameters ( $M_s$ ,  $t_s$ ,  $\beta$ ). We used the ‘‘SANN’’ method (Belisle, 1992), a Monte Carlo technique of solving optimization problems, with 10 million iterations to simultaneously solve the equations and optimize parameter values. Several sets of values for the parameters were generated using all 60 equations and subsets, allowing all three parameters to be free, assuming  $t_s$  to be 100, 150 and 200 Myr, and varying the time window within which the BHs had similar masses, the motivation being to obtain the most likely optimum value for  $\beta$ . Computations with  $t_s=150$  and 200 gave the largest RMS residuals and were rejected. A covariance was noted between  $t_s$  and  $\beta$ , in that an earlier  $t_s$  gave a somewhat lower  $\beta$  and vice versa. As suspected, subsets comprising BHs with masses within a narrower range of the mean value of  $2.5 \times 10^9 M_{\odot}$  or a narrower age range produced lower residuals. The ensemble of the solutions indicated that the most likely value for  $t_s$  was neither much less nor much more than 100 Myr. Finally,  $t_s = 100$  Myr ( $z \sim 30$ ) and the corresponding  $\beta \approx 14.6$  were adopted as the most likely optimum values.

Substituting these values of  $\beta$  and  $t_s$  in Eq.3, we get Eq.4A where age  $t$  is in Myr. And using the approximation  $1/t \propto (1+z)^{3/2}$  for high  $z$  (Bergström and Goobar, 2006), we can rewrite Eq.4A expressing a BH’s  $M_{\text{BH}}$  as a function of  $z$  as in Eq.4B. Note that Eq. 4A and 4B may yield slightly different results because of the approximation. Note also that Eq.4 does not depend on any material assumption or ad-hoc data selection.

$$M_{\text{BH}} = M_s \exp [14.6(t - 100)/t] \quad (4A)$$

$$M_{\text{BH}} = M_s \exp 14.6 [1 - (1 + z)^{3/2} / (1+30)^{3/2}] \quad (4B)$$

## 5. APPLICATION TO HIGH-Z SMBHs: LIMITS ON SEED SIZE

Figure 2 shows the seed mass  $M_s$  versus age  $t$  distribution for the 91 BHs in Fig.1 predicted using Eq.4. Figures 1&2 share identical  $M_{\text{BH}}$  symbols. Remarkably, the predicted  $M_s$  distribution in Fig.2 closely mimics the observed  $M_{\text{BH}}$  distribution in Fig.1. The 60 blue squares having similar  $M_{\text{BH}}$  have markedly similar  $M_s$ ; the red circles having smaller  $M_{\text{BH}}$  have correspondingly smaller  $M_s$ ; the red triangles with the largest  $M_{\text{BH}}$  have the largest  $M_s$ ; and the BHs range in  $M_{\text{BH}}$  over  $\sim 2.5$  orders of magnitude and so do their  $M_s$ . Figure 3 shows the predicted seed mass  $M_s$  versus BH mass  $M_{\text{BH}}$  for all 93 BHs including GNz11 and CEERS\_1019, the two red dots in the lower left corner of the figure. The symbols are the same as those in Figs. 1&2. The largest BH

in Fig.3 (#31 in Table A1) requires a seed mass  $M_s=(3\pm 1)\times 10^4 M_\odot$  for a  $2\sigma$  uncertainty in its mass. And those with masses  $1-5\times 10^9 M_\odot$  (blue squares in Fig.3) require seeds  $>10^3 M_\odot$  but  $<10^4 M_\odot$ . Of the 93 BHs, GNz11 and CEERS\_1019 are the smallest, requiring  $M_s \sim 20 M_\odot$  and  $\sim 53 M_\odot$  respectively, or a few to several tens of solar masses. Additionally, Eq.4 predicts that a seed of  $\sim 418 M_\odot$  formed at  $t_s=100\text{Myr}$  accounts for the mass of UHZ1 ( $z\sim 10.1$ ) estimated to be  $\sim 4\times 10^7 M_\odot$  by Natrajan et al. (2024), who concluded that a heavy seed of  $\sim 10^4 M_\odot$ , probably a DCBH, formed at  $t_s\sim 300\text{Myr}$  best fits its spectral data. If so, the value of  $\beta$  in Eq.3 for UHZ1 would be  $\sim 22.9$  and lead to the unacceptable conclusion that UHZ1 would have grown to  $\sim 9\times 10^{10} M_\odot$  by the age of a billion years, well exceeding the mass of the largest high- $z$  SMBH observed so far. We conclude that none of the three recently discovered AGN at  $z\geq 8.7$  require heavy seeds. Instead, their masses are accounted for with seeds formed at  $z=30$  ranging in  $M_s$  from a few tens to a few hundred solar masses.

Furthermore, we can place upper and lower limits on the size of seeds that formed at  $z\sim 30$ . The largest high- $z$  BH (#31, Table A1) was discovered  $\sim 10$  years ago, and the second largest (#59) more than two decades ago. In all likelihood, these BHs represent an upper limit on the size of SMBHs in the early universe. If so, we can conclude that the largest seeds formed at  $z\sim 30$  did not exceed  $(3\pm 1)\times 10^4 M_\odot$ , the seed mass required for the largest of the 93 SMBHs. Conversely, while we cannot place a strict lower limit on the size of seeds formed at  $z=30$ , we can conclude that it has to be  $<20 M_\odot$  based on the  $M_s$  required for GNz11, the smallest of the 93 high- $z$  SMBHs. Lastly, we note that Eq.4A predicts that the maximum size a BH can achieve via luminous accretion depends on its seed mass amounting to  $M_s$  times  $\text{Exp}14.6$  or  $\sim 2.2\times 10^6 M_s$ , which translates into  $(6.6\pm 2.2)10^{10} M_\odot$  for the empirically determined upper limit of  $M_s = (3\pm 1)\times 10^4 M_\odot$ , in excellent agreement with a probable theoretical limit of  $\sim 5\times 10^{10} M_\odot$  proposed by King (2016).



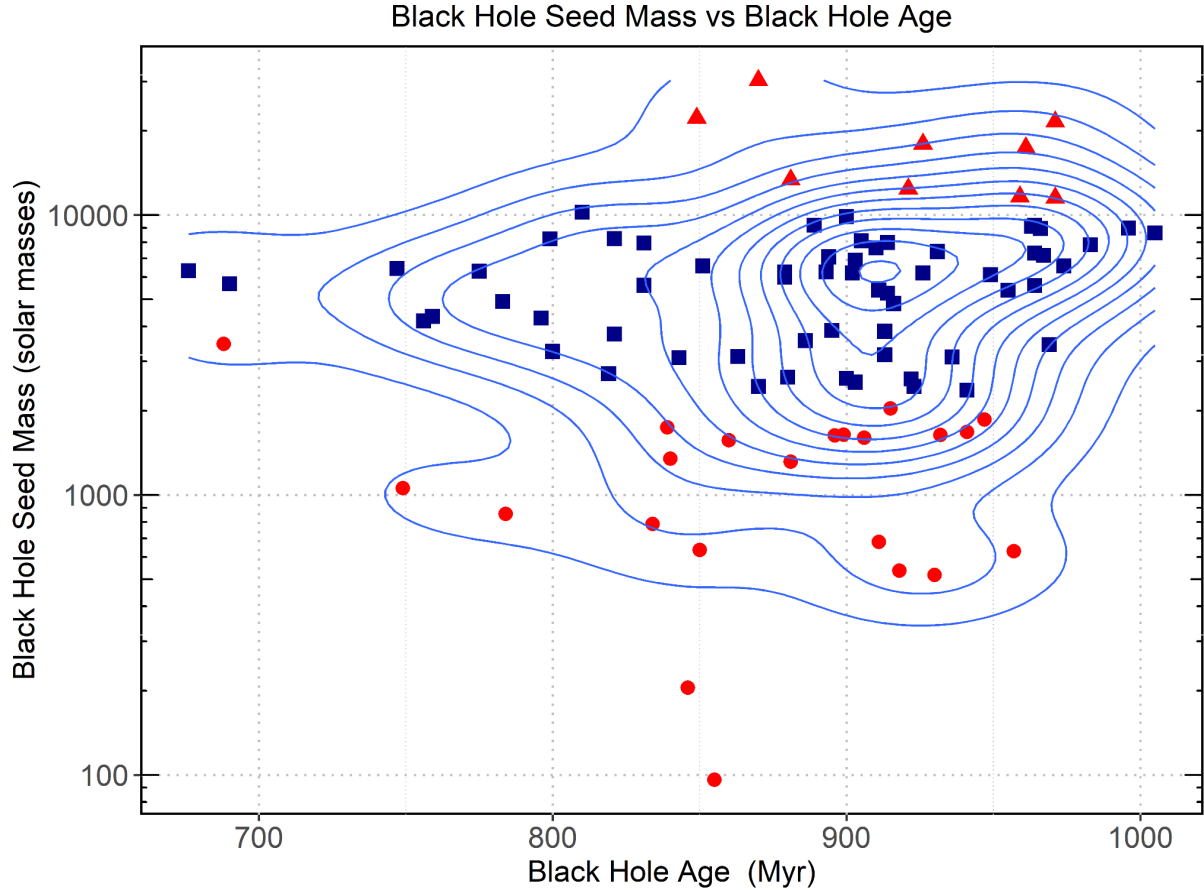


Fig.2: Seed mass  $M_s$  versus age  $t$  predicted by Eq.4 for the BHs in Fig.1. The symbols are the same as in Fig.1, differentiating BHs based on their  $M_{\text{BH}}$ . The distribution of  $M_s$  mimics the distribution of  $M_{\text{BH}}$  in Fig.1, and so do the density contours.

## 6. APPLICATION TO LOWER-Z SMBHs: SEED CLASSIFICATION

We applied Eq.4B to the 132,446 AGN at  $z < 2.4$  (Kozłowski, 2027) to test the universality of its applicability and derive the size distribution of the seeds. The resulting  $M_s$  are sorted into narrow bins, and the number in each mass bin is shown in Table 1. In most cases, the uncertainty in  $M_{\text{BH}}$  is unknown but is of little importance except when there are relatively few seeds in a bin. Of the total population of BHs, 540 BHs have  $\geq 10^{10} M_{\odot}$ , and none of their predicted  $M_s$  exceed the preceding empirically established upper limit of  $(3 \pm 1) \times 10^4 M_{\odot}$  except possibly in 5 cases (Table 1) and that too by a factor of  $< 1.7$  in the worst case. However, the uncertainty in the  $M_{\text{BH}}$  of these 5 BHs is unknown. In particular, we note that the predicted  $M_s$  for TON 618 at  $z=2.219$  and  $4.07 \times 10^{10} M_{\odot}$  (Xue Ge et al., 2019), which is often cited as the most massive BH observed to date, is identical to that of the largest high- $z$  BH (#31). At the lower end of the  $M_s$  spectrum, the results (Table 1) show that 88 BHs have predicted  $M_s$  between  $5\text{-}10 M_{\odot}$  and  $\sim 1000$  between

10-20 $M_{\odot}$  in agreement with the lower limit of  $M_s$  expected from the high- $z$  data. This striking agreement on the upper and lower limits on the size of seeds deduced from 2 entirely different sets of data covering different cosmic periods cannot simply be fortuitous and testifies to the validity and universal applicability of Eq.4.

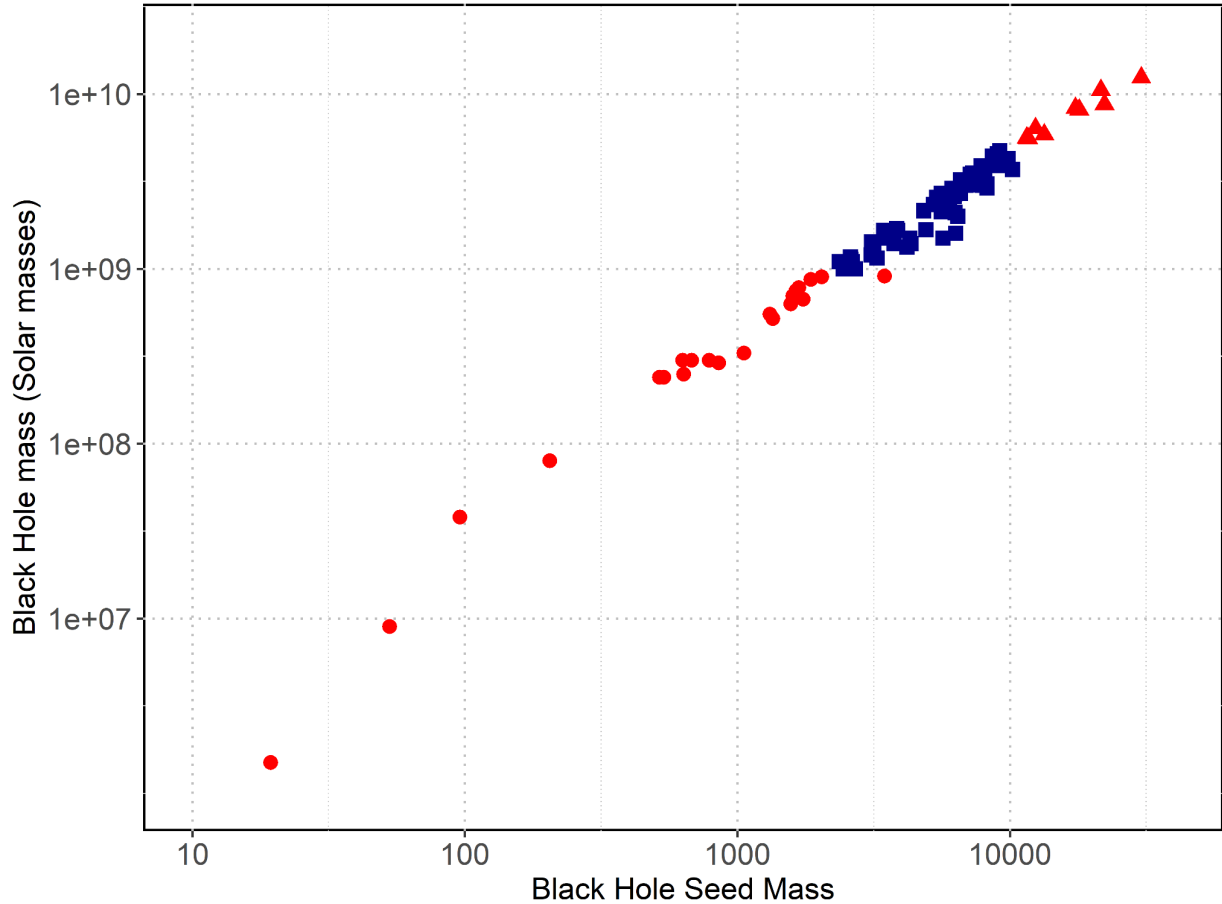


Fig.3. Seed mass  $M_s$  versus black hole mass  $M_{BH}$  on a log-log scale for the 91 BHs in Fig.1 and GNz11 and CEERS\_1019 ( $M_{BH} < 1e+07M_{\odot}$ , bottom left corner). The symbols are identical to those in Figs.1&2. The  $M_s$  for GNz11 and CEERS\_1019 are respectively  $\sim 20M_{\odot}$  and  $\sim 53M_{\odot}$ . The  $M_s$  for BHs with  $M_{BH}$   $1-5 \times 10^9 M_{\odot}$  (blue squares) have  $10^3 M_{\odot} < M_s < 10^4 M_{\odot}$ , and the  $M_s$  for the largest BH is  $\sim 3 \times 10^4 M_{\odot}$ .

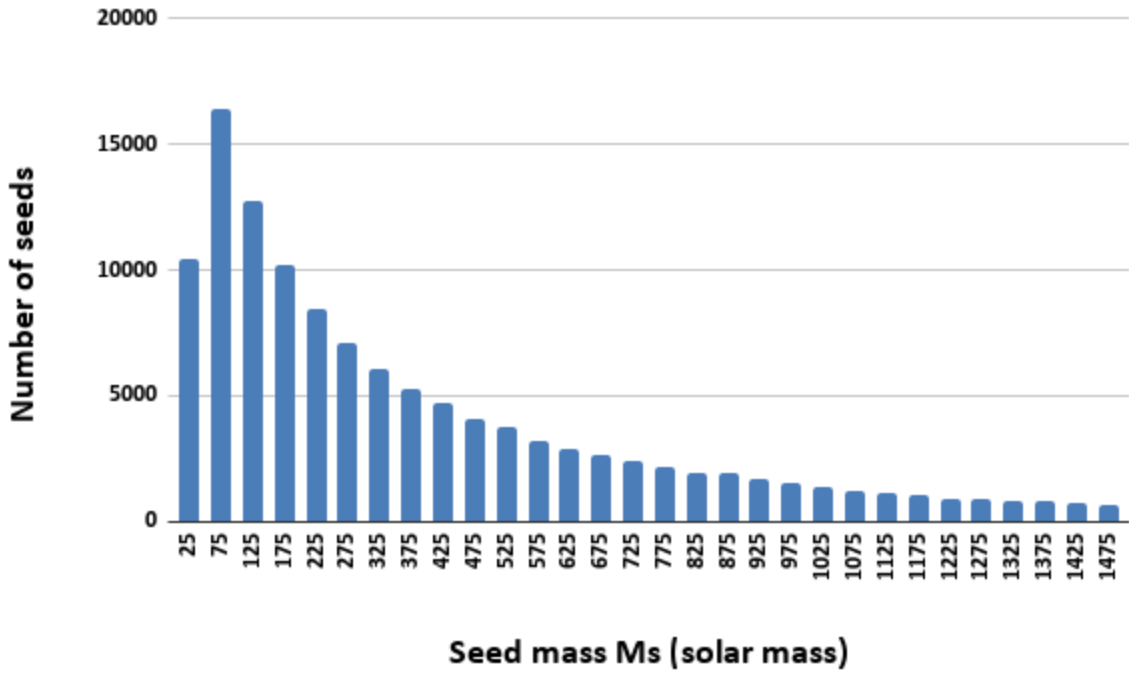


Fig.4. Histogram showing the number of seeds in bins of  $50M_{\odot}$  (solar masses) for 90% of 132,446 SMBHs at  $z < 2.4$  predicted by Eq.4B. Each bar is plotted at the central mass value of the bin. The distribution of the rest at  $M_s > 1500M_{\odot}$ , not plotted because of their small numbers, is given in Table 1. Note the initial increase in seed counts before the monotonic decrease, the significance of which is discussed in the text.

The seed counts in Table 1 indicate that  $\sim 90\%$  of the seeds have  $M_s \leq 1.5 \times 10^3 M_{\odot}$ . The histogram in Fig.4 shows their mass distribution, where each bin has the same size of  $50M_{\odot}$  and is identified by the central value of  $M_s$  in the bin. The remaining 10% are not plotted because of their small numbers but follow the same pattern, decreasing asymptotically towards zero at  $M_s \sim 3 \times 10^4 M_{\odot}$ , the upper limit of seed mass. Table 1, however, gives the number of seeds in different bin sizes for the remaining 10% of AGN that amount to less than the number in the single bin of  $50\text{-}100M_{\odot}$  centered at  $M_s = 75M_{\odot}$  in Fig.4. The seeds in Fig.4 range in  $M_s$  from a low of  $\sim 5M_{\odot}$  to a high of  $\sim 1.5 \times 10^3 M_{\odot}$  and can be designated as light to intermediate-size seeds based on their universally accepted size classification. They constitute an overwhelming majority of the seeds. In contrast, seeds  $\geq 10^4 M_{\odot}$  or heavy seeds constitute a small number totaling  $\sim 210$  or  $\sim 0.16\%$  of the seed population (see Table 1). Furthermore, the distribution in Fig.4 shows a monotonic systematic decrease in the number of seeds without any hiatus or break, preceded by an initial increase in seed counts.

**Table 1: Seed counts**

<b>Ms</b>	<b>Count</b>	<b>Ms</b>	<b>Count</b>	<b>Ms</b>	<b>Count</b>	<b>Ms</b>	<b>Count</b>
5-10	88	200-250	8,473	800-850	1,963	1400-1450	745
10-20	1014	250-300	7,063	850-900	1,913	1450-1500	703
20-30	2394	300-350	6,063	900-950	1,721	1500-1800	3383
30-40	3332	350-400	5,241	950-1000	1,528	1800-2200	2775
40-50	3605	400-450	4,700	1000-1050	1,419	2200-2700	2217
50-60	3595	450-500	4,064	1050-1100	1,231	2700-3400	1747
60-70	3481	500-550	3,728	1100-1150	1,161	3400-4200	1051
70-80	3261	550-600	3,226	1150-1200	1,081	4200-6400	1097
80-90	3110	600-650	2,910	1200-1250	944	6400-10000	462
90-100	2979	650-700	2,672	1250-1300	926	10000-14000	144
100-150	12,739	700-750	2,385	1300-1350	843	14000-30000	61
150-200	10,159	750-800	2,217	1350-1400	829	>30000	5

Ms seed mass (solar mass). The count is the number of seeds in a bin. Bin size varies.

Rather than reviewing the numerous simulations of BH seed formation reported in the literature, we shall attempt to identify those that best match the distribution of seeds in Fig.4 and Table 1. Light seeds are thought to have formed from the collapse of massive metal-free first or Pop III stars (Madau and Rees, 2001; Johnson and Bromm, 2007). Our finding that the seeds formed around  $z=30$  is consistent with the notion that the first stars formed at  $z\sim 30$  (e.g., Couchman and Rees, 1986). Their stellar mass functions derived from simulations range from  $<10M_{\odot}$  to  $\sim 1000M_{\odot}$  (e.g., Hirano et al., 2014; Hosokawa et al., 2015; Stacy et al., 2016). These simulations have been reviewed by Latif and Ferrara (2016), who concluded that the results suggest that the typical mass of Pop III stars is  $\sim 100M_{\odot}$  except for a few cases of  $1000M_{\odot}$ . As noted earlier, Fig.4 shows that the number of seeds decreases systematically as Ms increases except at the beginning or low end of the Ms spectrum. A closer examination reveals that at the

low end of the  $M_s$  spectrum, the number of seeds increases exponentially and reaches a plateau before decreasing monotonically. The counts in Table 1 show that the number of seeds increases from 88 having  $M_s \leq 10M_\odot$  to 1014 and 2395 in the successive bins of  $10\text{-}20M_\odot$  and  $20\text{-}30M_\odot$  and reaches a plateau of  $\sim 3600$  in the bins of  $40\text{-}50M_\odot$  and  $50\text{-}60M_\odot$ ; after which the counts decrease slowly but monotonically. This predicted mass distribution of light seeds resembles the stellar-mass distribution shown in Fig.5 of Hirano et al.(2014) derived from hydrodynamic simulations. Their histogram of 100 first stars accreting at lower rates, identified by red and blue colors in Fig.5, shows that the number of stars increases  $>10$ -fold from 1 with a mass  $<10M_\odot$  to 11 with a mass of  $\sim 40M_\odot$ , after which the number of stars decreases almost monotonically to 1 at  $\sim 1000M_\odot$ . However, as noted by them, most stars have masses from a few tens to a few hundred solar masses, consistent with the distribution of seeds in Table 1 and Fig.4 that show that  $\sim 60\%$  of the seeds with  $M_s < 1000M_\odot$  have masses between  $10M_\odot$  and  $300M_\odot$  and  $\sim 70\%$  have  $<400M_\odot$ . Thus, there is a good agreement between the mass distribution of the first stars derived from simulations and the empirically derived mass distribution of seeds that presumably formed from the collapse of the first stars. In the simulation, however, there is a marked low in the number of stars immediately following the maximum, whereas in Fig.4, there is no such hiatus. Later, we provide an explanation reconciling this dichotomy.

Most likely, there is an overlap in the sizes of light and intermediate seeds. There is, however, no decipherable change, hiatus, or break in the asymptotic decrease in the number of seeds as  $M_s$  increases in Fig.4. Thus, it is difficult, if not impossible, to define a strict  $M_s$  boundary in Fig.4 between the light and intermediate seeds. In contrast to light seeds, intermediate-size seeds are thought to have formed either via runaway collisions of stars in dense stellar clusters (Portegies et al., 2004; Freitag et al., 2006; Mapelli, 2016) or by the hierarchical merger of BHs in stellar clusters (Davies et al., 2011; Lupi et al., 2014). Devecchi et al. (2012) performed simulations simultaneously investigating the formation of Pop III remnants and BHs via runaway collisions in nuclear star clusters. The results in their Fig.4 show that the BHs formed via runaway collisions decrease in number by a factor of  $\sim 5$  as BH mass increases from  $\sim 400M_\odot$  to  $\sim 3000M_\odot$ , qualitatively in agreement with the decrease in the number of seeds as  $M_s$  increases in Fig.4 and Table 1 of this study. Note that  $\sim 97\%$  of the seeds in Table 1 have  $M_s < 3000M_\odot$ . Hence, intermediate-size seeds formed via runaway collisions of stars and light seeds formed by the collapse of the first stars could together account for the entire population of seeds in Table 1 except  $\sim 3\%$ . There is, however, a potential problem. The seeds in Table 1 were deduced to have formed at  $z \sim 30$ , whereas the intermediate-size BHs via runaway collisions of stars in the simulations formed at  $z \sim 15$ , a delay of  $\sim 150$  Myr.

On the other hand, Lupi et al. (2014) explored gas-induced runaway merger of BHs dubbed the GIRM model, following the Davies et al. (2011) prescription of hierarchical growth of BHs in dense stellar clusters. The results in their Fig.7 also show that the number of BH seeds formed

via GIRM decreases dramatically as the seed mass increases from  $\sim 400M_{\odot}$  to  $\sim 2000M_{\odot}$ . Most of the BHs in their simulations also formed at  $z < 20$ . They, however, point out that GIRM requires some degree of metal pollution of the intergalactic medium from the explosions of the massive Pop III stars and that the “GIRM channel does not pose any constraint on the level of the metallicity of the parent halo, and hence on the time of formation, provided Pop III stars have enhanced the metallicity above a threshold.” If so, this mechanism and that for the formation of light seeds could together also account for at least 94% of the seed population in Table 1. This mechanism has the advantage that the Pop III remnants could provide the degree of metal pollution required in the simulations. Alternatively, the formation of intermediate-size BHs could have resulted from the merger of Pop III remnants, but whether this is a realistic possibility can be ascertained by simulations, a task beyond the scope of this paper. If possible, it would explain why there is no hiatus or break in the mass distribution of seeds in Fig.4 and Table 1 and why intermediate-size follow the same asymptotically decreasing trend as the light seeds. Furthermore, the probability of forming larger seeds from a given population of stellar seeds would systematically decrease as seed mass increases, consistent with the systematic decrease in seed counts as  $M_s$  increases observed in Fig.4 and Table 1

It is remarkable that in the preceding simulations, whether involving runaway collisions of stars or runaway mergers of BHs, the resulting mass spectrum of intermediate-size seeds is strikingly similar, ranging from  $\sim 400M_{\odot}$  to  $\sim 2000M_{\odot}$  or  $3000M_{\odot}$ . Thus, based on the results of these simulations and the preceding discussion on the distribution of seeds in Fig.4 in the context of the results of the simulations by Hirano et al. (2014), we can classify seeds  $< 400M_{\odot}$  as light seeds predominantly formed from the collapse of first stars and those between  $400M_{\odot}$ - $3000M_{\odot}$  as predominantly intermediate size. Based on this working classification, we conclude that of the 132,446 seeds in Table 1,  $\sim 58\%$  are light, and  $\sim 39.4\%$  are intermediate-size. The remaining  $< 3\%$  or 3681 have  $M_s$  between  $\sim 3 \times 10^3 M_{\odot}$  -  $3 \times 10^4 M_{\odot}$  (dubbed heavier seeds in contrast to heavy), of which only 210 have  $M_s \geq 10^4 M_{\odot}$  that could strictly be classified as heavy seeds. Moreover, these relatively few heavy seeds have  $M_s \leq 3 \times 10^4 M_{\odot}$  or at the lower end of the expected mass spectrum of  $10^{4-6} M_{\odot}$  (see Volonteri et al., 2022) for heavy seeds thought to have formed by the DCBH mechanism. The implication is that the DCBH mechanism did not play an essential role in seed formation. Moreover, the ‘number of “heavier” seeds decreases as  $M_s$  increases (see Table 1), following the same pattern as the light to intermediate-size seeds in Fig.4, which suggests that the same mechanism responsible for forming intermediate-size seeds may also account for the rare formation of heavy seeds. Apropos, Davies et al. (2011) have proposed that seeds as large as  $10^5 M_{\odot}$  can be formed by hierarchical growth of BHs in dense stellar clusters. We conclude, therefore, that the DCBH mechanism is not required while not closing the possibility that a relatively small number may have formed by the DCBH mechanism.

## 7. ACCRETION RATE, EDDINGTON RATIO, RADIATIVE EFFICIENCY

Having established the universal applicability of Eq. 4, we can use its derivative to gain insights into the growth history of SMBHs. Differentiating  $M_{\text{BH}}$  ( $dM_{\text{BH}}/dt$ ) in Eq.4A, we get Eq.5 expressing a BH's instantaneous accretion rate  $\dot{M}$  ( $M_{\odot}/\text{year}$ ) as a function of  $M_{\text{BH}}$  and  $t$  (Myr) or as a function of  $z$  using the approximation  $1/t \propto (1+z)^{3/2}$  (Bergström, and Goobar, 2006)

$$\dot{M} (M_{\odot}/\text{yr}) = 14.6 \times 10^{-4} M_{\text{BH}} / t^2 \simeq 4.96 \times 10^{-12} M_{\text{BH}} (1+z)^3 \quad (5)$$

Note that in Eq.5, the instantaneous accretion rate per unit BH mass  $\dot{M}/M_{\text{BH}}$  is directly proportional to  $(1+z)^3$  and hence decreases as  $z$  decreases, fulfilling the requirement in the section on the theoretical basis that  $\dot{M}/M_{\text{BH}}$  decrease as  $z$  decreases. Furthermore, in the Standard Cosmological Model, the ambient gas density scales as  $(1+z)^3$ , and hence, the accretion rate  $\dot{M}$  scales as the product of a BH's mass  $M_{\text{BH}}$  and the ambient gas density.

Eq.5 can be applied to any actively accreting BH to ascertain its instantaneous accretion rate  $\dot{M}$ . For example, Eq.5 yields  $\dot{M} \sim 0.012 M_{\odot}/\text{yr}$  for GNz11 at  $z=10.6$ ,  $\sim 24 M_{\odot}/\text{yr}$  for the largest high- $z$  SMBH at  $z=6.3$  (#31), and  $\sim 6.6 M_{\odot}/\text{yr}$  for TON 618 at  $z=2.219$ . Moreover, by substituting  $M_{\text{BH}}$  in Eq.5 with its expression in Eq.4B, we get Eq.6 expressing  $\dot{M}$  as a function of a BH's seed mass  $M_s$  and redshift  $z$ .

$$\dot{M} = 4.96 \times 10^{-12} M_s (1+z)^3 \exp 14.6 [1 - (1+z)^{3/2} / (1+30)^{3/2}] \quad (6)$$

Using Eq.6. one can infer the history of a BH's accretion rate from its inception at  $z=30$  to any redshift  $z$  by plugging in Eq.6 the BH's seed mass  $M_s$  inferred from Eq.4B. Figure 5 shows the accretion rate history of a seed of unit solar mass. Initially,  $\dot{M}$  increases exponentially and reaches a broad peak between  $z=8.5$  and 6, beyond which it decreases slowly but monotonically towards  $z=0$ . Note that the broad peak from  $z=8.5-6$ , during which a BH has the highest accretion rate and hence likely the highest luminosity, incidentally coincides with the epoch during which reionization is thought to have occurred (e.g., Grazian et al., 2018). However, exploring to what extent BHs during this period (the mass function of which can be inferred using the results in Table 1 and Eq.4) may have contributed to the reionization is beyond the current scope of this paper. Notwithstanding this sidebar, we note that two competing factors, namely the increase in a BH's mass or gravitational reach as it ages and the decrease in the ambient gas density as  $z$  decreases, determine a BH's  $\dot{M}$  at any instant of its life. Hence, the results in Fig.5 suggest that initially the BH's mass or its gravitational reach increases faster than the decrease in the ambient gas density. The two competing factors reach a parity near  $z \sim 7$ , after which the decline in gas density dominates over the gradual increase in the BH's mass and  $\dot{M}$

steadily decreases. For example, Eq.4B predicts that the seed of TON 618, one of the largest SMBHs, grew from  $M_s = 3.03 \times 10^4 M_\odot$  by  $\sim 5.5$  orders of magnitude to  $\sim 9.8 \times 10^9 M_\odot$  by  $z=7$  and after that by a factor of  $\sim 4$  until its present  $z=2.219$ . And Eq.6 predicts that its accretion rate changed from  $0.08 M_\odot/\text{yr}$  at  $z=25$  to  $24.6 M_\odot/\text{yr}$  at  $z=7$  and  $6.6 M_\odot/\text{yr}$  at  $z=2.219$ .

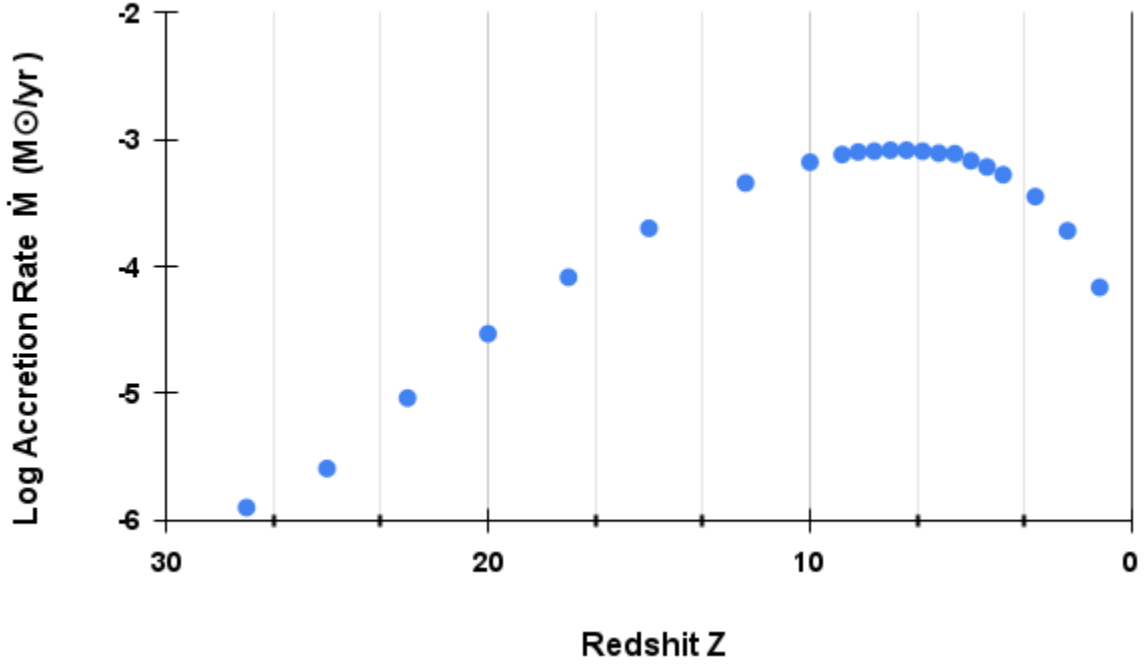


Fig.5: Log of instantaneous accretion rate  $\dot{M}$  for a BH seed of unit (solar) mass  $M_\odot$  as a function of redshift  $z$  starting at  $z \sim 30$  based on Eq.6. Initially  $\dot{M}$  increases exponentially, reaches a broad peak between  $z \sim 8.5$  and  $6$  with a maximum at  $z \sim 7$ , and steadily decreases after that towards  $z=0$ . Note that the timing of the broad peak from  $z=8.5-6$  coincides with the epoch during which reionization is thought to have occurred.

Using Eq.5, we can also define the Eddington ratio  $\lambda$ , or the ratio of a BH's bolometric luminosity  $L_{\text{bol}}$  to its Eddington luminosity ( $L_{\text{EDD}}$ ), as a function of  $z$  and radiative efficiency  $\epsilon$ .  $L_{\text{bol}} = (\dot{M}c^2) \epsilon / (1 - \epsilon)$  where  $c$  is the velocity of light and  $\dot{M}$  the accretion rate; and  $L_{\text{EDD}} = 1.3 \times 10^{38} M_{\text{BH}}$  in ergs/s with  $M_{\text{BH}}$  in solar mass. Radiative efficiency  $\epsilon$  is conventionally defined relative to the mass inflow rate, such as the Bondi rate, and a BH's  $\dot{M}$  is smaller by  $(1 - \epsilon)$ . Thus, by Substituting  $\dot{M}$  from Eq.5 into the definition of  $L_{\text{bol}}$ , we get Eq.7 expressing the Eddington ratio  $\lambda$  as a function of a BH's redshift and radiative efficiency.

$$\lambda = 2.18 \times 10^{-3} (1 + z)^3 \epsilon / (1 - \epsilon) \quad (7)$$



Equation 7 implies that  $\lambda$  decreases as  $z$  decreases, irrespective of whether  $\epsilon$  depends on  $z$ . This implication is validated by empirical evidence. Using Kozłowski's data for the tens of thousands of AGNs at  $z < 2.4$ , Aggarwal (2024) unambiguously showed that  $\lambda$  decreases as  $z$  decreases. Moreover, Eq.7 implies that of 2 BHs at similar redshifts, the BH with a higher  $\lambda$  is less efficient (higher  $\epsilon$ ) in accreting gases than the one with a lower  $\lambda$ . This implication is also consistent with the finding by Aggarwal (2024) that larger BHs have lower  $\lambda$  and are more efficient than smaller BHs. And, using the Bondi prescription for spherically symmetric accretion and observational data for temperature and density profiles near BHs in galaxies M87, NGC 3115, and NGC 1600, Aggarwal (2024) derived a scaling relation for  $\lambda$  identical in form to the above Eq.7. Thus the substantiations of the implications of Eq.7 and the similarity between scaling relations for  $\lambda$  derived from 2 different prescriptions and entirely different data sets are further evidence of the validity and universal applicability of Eq.4 from which Eq.7 is derived.

A BH's radiative efficiency  $\epsilon$  can be inferred from Eq.7, knowing its  $\lambda$  or bolometric luminosity. Unfortunately, determining  $\lambda$  is prone to multiple errors arising from uncertainties in the BH's mass, its luminosity, and the correction factor used to get its bolometric luminosity. However, by applying Eq.7 to large groups of similarly situated BHs at markedly different redshifts, we can garner insights into the dependence of  $\epsilon$  on  $z$ . For example, Shen et al. (2019) list 50 BHs, most of which have  $1-4 \times 10^9 M_{\odot}$  with redshifts close to 6 and a mean  $\lambda \sim 0.32$ , whereas a large group of similar-size BHs at  $z \sim 1$  in Kozłowski's catalog have a mean  $\lambda = 0.03$ . Applying Eq.7 to the two groups, one gets  $\epsilon \sim 0.63$  for the lower and  $\epsilon \sim 0.3$  for the higher- $z$  group, a decrease by a factor of 2 despite a  $\sim$  ten-fold increase in  $\lambda$  from  $z \sim 1$  to  $z \sim 6$ . The implication is that  $\epsilon$  decreases as  $z$  increases, consistent with a similar finding by Aggarwal (2024).

The vast majority of the values of  $\lambda$  for the BHs in Table A1 and reported by Shen et al. (2019) and Kozłowski (2017) are  $< 1$ , all of which are at  $z < 7.7$ . GNz11 is a notable exception that deserves special attention because it is the highest- $z$  AGN observed so far and is inferred to be accreting by as much as 5.5 times the Eddington rate (Maiolino et al., 2024). If so, Eq.7 predicts a radiative efficiency  $\epsilon$  of  $\sim 0.59$  that ostensibly is exceptionally high, especially since  $\epsilon$  has been shown to decrease as  $z$  increases. And, it would imply that GNz11 is a relatively poor accreter, accreting only  $\sim 41\%$  of the gas inflow. Interestingly, a lower  $\lambda$  would make GNz11 a more efficient accreter. For example,  $\lambda = 1$  would yield  $\epsilon = 0.227$ , making GNz11  $\sim 2.6$  times more efficient than if its  $\lambda = 5.5$ . Its  $\lambda$  is probably highly overestimated. We note that Schneider et al. (2023) estimated a significantly lower  $\lambda$  of 2-3 for it, and Bhatt et al. (2024) found that the probability of observing a BH at  $z \sim 10-11$  accreting with  $\lambda \sim 5.5$  in the volume surveyed by JWST is  $< 0.2\%$ .

Given that  $\lambda$  is prone to large uncertainties and hence a poor predictor of whether a BH is accreting above the Eddington limit, we propose instead the following. As noted earlier, the

growth efficiency parameter  $\Upsilon$  defined by Eq.2 has a value of 1 for a BH accreting at the Eddington limit ( $\lambda=1$ ) with a radiative efficiency  $\varepsilon=0.1$  (its canonical value) and a duty cycle  $\delta=1$ . For  $\delta=1$ , a value of  $\Upsilon > 1$  implies that the BH is either accreting above the Eddington limit ( $\lambda > 1$ ) or that its  $\varepsilon < 0.1$ . Substituting  $\lambda$  from Eq.7 into Eq.2 (the definition of  $\Upsilon$ ), one gets  $\Upsilon \sim 2.4 \times 10^{-4} \delta (1+z)^3$  for the instantaneous value of  $\Upsilon$  as opposed to its value averaged over a BH's life span in Eq.1. Shankar et al. (2010) found that in their sample of AGNs, the duty cycle  $\delta$  increased with  $z$  reaching  $\sim 0.9$  at  $z=6$ . It is likely, therefore, that  $\delta \sim 1$  at even higher redshifts. Hence, at very high redshifts, the instantaneous value of  $\Upsilon \sim 2.4 \times 10^{-4} (1+z)^3$  is solely a function of the gas density. For  $z > 15$ ,  $\Upsilon > 1$ , implying that either  $\lambda > 1$  or  $\varepsilon < 0.1$  at those high redshifts. Therefore, it is likely that during the first  $\sim 150$  Myrs ( $z \geq 15$ ) of its life, a BH experienced super-Eddington accretion or its radiative efficiency was  $< 0.1$ . This finding is consistent with the suggestion by Wythe and Loeb (2012) and Pacucci et al. (2015) that super-Eddington accretion is possible when a BH is embedded in sufficiently dense gas that renders the radiation pressure less effective. For example, in the Standard Model, the ambient gas density at  $z=20$  is 27 times greater than at  $z=6$ .

## 8. CONCLUSIONS

Prompted by insights derived from a deconstruction of the so-called Salpeter relation (Eqs.1-3), we analyzed the mass versus age distribution of 91 high- $z$  SMBHs (Fig.1) that resulted in the formulation of Eq.4, the foundation on which the findings and conclusions of this paper are based. It describes a BH's mass  $M_{\text{BH}}$  as a function of its age  $t$  or redshift  $z$ , from which the BH's seed mass  $M_s$  can be determined. It was extensively tested throughout the paper by verifying its implications and predictions. It, together with its derivatives (Eqs.5-7), comprises a set of powerful tools to decipher the origins, growth, and properties of SMBHs.

We applied Eq.4 to 93 high- $z$  ( $> 5.6$ ) and 132,446 AGNs at  $z < 2.4$  listed by Kozłowski (2017). The resulting mass distributions of seeds (Figs. 2,3,4, and Table 1) show that the masses of the smallest to the largest actively accreting SMBHs observed to date are accounted for by seeds formed at  $z \sim 30$  ranging in  $M_s$  from a low of  $\sim 5 M_{\odot}$  to a maximum of  $(3 \pm 1) \times 10^4 M_{\odot}$ . In particular, the  $M_{\text{BH}}$  of GNz11, CEERS\_1019, and UHZ1), the three highest redshift ( $z=8.7-10.6$ ) AGNs discovered recently, are accounted for by stellar-mass seeds ranging from a few tens to a few hundred solar masses. Specifically, the results exclude the possibility that the seed of UHZ1 was heavy, presumably a DCBH, as postulated by Natrajan et al. (2024). Equation. 4A places an upper limit of  $\sim 2.2 \times 10^6 M_s$  on the mass a seed can accrete via luminous accretion, which translates into  $(6.6 \pm 2.2) \times 10^{10} M_{\odot}$  for  $M_s = (3 \pm 1) \times 10^4 M_{\odot}$  in agreement with a theoretical limit proposed by King (2016) and with the size of the largest SMBHs observed to date.

The mass distribution of seeds shown in Fig.4 and Table 1 was analyzed and compared with the simulated mass functions of first stars and intermediate-size BHs reported in the literature. Based on this comparative analysis, we classified the seed population into three broad categories depending on seed size and the likely mechanism for its formation, fully recognizing that there is probably overlap between the categories. Seeds  $\leq 400M_{\odot}$  were classified as light seeds predominantly formed from the collapse of massive metal-free first stars (Madau and Rees, 2001; Johnson and Bromm, 2007). Their observed mass distribution in Fig.4 and Table 1 resembles the mass function in simulations of first stars by Hirano et al. (2014). Seeds ranging from  $400M_{\odot}$ - $3 \times 10^3 M_{\odot}$  were classified as intermediate size formed either by runaway collisions of stars in dense stellar clusters (Portegies et al., 2004; Freitag et al., 2006) or by the hierarchical growth via runaway mergers of BHs (Davies et al., 2011; Lupi et al., 2014). Their observed mass distribution (Fig.4 and Table 1) resembles the mass functions of BHs in simulations of runaway collisions of stars by Devecchi et al. (2012) and in gas-induced runaway merger of BHs by Lupi et al. (2014). Light seeds constitute  $\sim 58\%$  and intermediate size  $\sim 39.4\%$  of the population in Table 1. The remaining  $<3\%$  ranging in mass from  $\sim 3 \times 10^3 M_{\odot}$  to  $\sim 3 \times 10^4 M_{\odot}$  are dubbed heavier seeds in contrast to the classical heavy seeds ( $10^{4-6} M_{\odot}$ ) thought to be DCBHs.

Of the 2 mechanisms for intermediate-size seeds, the hierarchical growth of BHs via runaway mergers is the more likely. In the Devecchi et al. (2012) simulations, the BHs formed at  $z \sim 15$  or significantly later than at  $z \sim 30$ ; whereas there is no such time restriction for the runaway merger of BHs as pointed out by Lupi et al. (2024). Furthermore, if the hierarchical growth occurred through the merger of Pop III remnants instead of new BHs formed at a later time, it would explain why light and intermediate-size seeds formed almost concurrently at  $z \sim 30$ , why the two follow the same asymptotically declining trend as seed mass increases with no hiatus in the distribution of seed sizes as observed in Fig.4, and why light seeds outnumber intermediate-size seeds. Of the heavier seeds, only a minuscule number (210) have  $> 10^4 M_{\odot}$  and that too at the lower end of the presumed sizes of DCBHs, which led us to conclude that the DCBH mechanism did not play a significant role and propose that the heavier seeds could also have formed via the merger of light to intermediate-size seeds. Apropos, Davies et al. (2011) postulated that BHs as large as  $10^5 M_{\odot}$  can form via runaway merger of BHs. In summary, the entire population of seeds in Table 1 could be Pop III remnants and larger BHs resulting from their hierarchical growth via runaway mergers under appropriate conditions. One such condition could be the inflow of gases as in the simulations by Lupi et al. (2014).

Equation 5 gives a BH's instantaneous accretion rate as a function of its mass  $M_{\text{BH}}$  and age  $t$  or redshift  $z$ . Eq.6 gives the same in terms of its seed mass  $M_s$  (inferred from Eq.4) and  $z$ . For example, Eq. 5 predicts an accretion rate of  $\sim 0.012 M_{\odot}/\text{yr}$  for GNz11, the smallest ( $\sim 1.5 \times 10^6 M_{\odot}$ ) high- $z$  (10.6) AGN;  $\sim 24 M_{\odot}/\text{yr}$  for the largest ( $\sim 1.24 \times 10^{10} M_{\odot}$ ) high- $z$  (6.3) SMBH; and  $6.6 M_{\odot}/\text{yr}$  for TON 618 at  $z \sim 2.22$  arguably the largest ( $4.07 \times 10^{10} M_{\odot}$ ) AGN observed to date.

Figure 5 illustrates the change in a BH's  $\dot{M}$  with  $z$  from its inception as a seed at  $z \sim 30$  to the present. Initially,  $\dot{M}$  increases exponentially and reaches a broad plateau between  $z=8.5-6$ , after which it decreases monotonically. Two factors, namely the increase in a BH's gravitational reach as its mass increases and the decrease in gas density as  $z$  decreases, modulate the accretion rate as the BH ages. A BH's mass increases by  $\sim 6$  orders of magnitude in the first billion years and only by a factor of  $\sim 4$  in the next  $\sim 12.8$  billion years. Also, we noted that the timing ( $z = 8.5-6$ ) of the maximum accretion rate in a BH's history coincides with the epoch when reionization is thought to have occurred.

Equation 7 expresses the Eddington ratio  $\lambda$  as a function of a BH's  $z$  and radiative efficiency  $\epsilon$ . It implies that  $\lambda$  decreases as  $z$  decreases, an implication substantiated by unambiguous empirical evidence (see Aggarwal, (2024)). Furthermore, a BH's radiative efficiency  $\epsilon$  can be determined using Eq.7 from its  $\lambda$ . We, however, stressed that  $\lambda$  is prone to large errors resulting from numerous uncertainties (see text), and hence Eq.7 should be used with caution. Nevertheless, using  $\lambda$  data for two large groups of similar-size BHs at two different redshifts, we showed that  $\epsilon$  is significantly lower for the higher- $z$  group even though its  $\lambda$  is substantially higher. The implication is that  $\epsilon$  increases as  $z$  decreases or that a BH becomes less efficient in accreting gases as it ages, which suggests that  $\epsilon$  is an inverse function of the ambient gas density consistent with the Wythe and Loeb (2012) and Pacucci et al. (2015) suggestion that the radiation pressure is less effective when a BH is embedded in dense gas. Finally, applying Eq.7 to Eq.2, we inferred that at redshifts  $>15$ , the radiative efficiency is significantly  $< 0.1$  its canonical value or that  $\lambda > 1$ , which suggests that SMBH's may have experienced super-Eddington accretion for a short period of  $\sim 150$  Myr from the inception of their seeds at  $z \sim 30$ .

**ACKNOWLEDGMENTS:** I thank Manuel Chirouze for solving the equations using the SANN method, drafting the figures, and suggesting using density contours in Figs. 1&2. Fabio Pacucci of the Center of Astrophysics at Harvard critically reviewed an advance copy of this article. I thank him for his review and helpful suggestions.

**DATA AVAILABILITY:** No new data were generated in this study.

**ETHICS DECLARATION** The authors declare no competing interests.

## REFERENCES

- Aggarwal, Y., 2204, MNRAS. 530, 1512-1515  
Barkana R., Loeb A., 2001, Phys. Rep., 349, 125  
Begelman M. C., Volonteri M., Rees M. J., 2006, MNRAS, 370, 289  
Belisle, C.J.P., 1992, J Applied Probability, 29 885-895  
Bergström L., and Goobar I., 2006, Cosmology and Particle Astrophysics, Springer 77.  
Bhatt, M. et al., 2024, A&A, 686, A141

Bondi, H., On the spherically symmetric accretion. *MNRAS*,. 112, 195 (1952).  
Bromm V., Loeb A., 2003, *ApJ*, 596, 34..  
Couchman, H. M. P., & Rees, M. J. 1986, *MNRAS*, 221, 53  
Davies M. B., Miller M. C., Bellovary J. M., 2011, *ApJ*, 740, L42  
Devecchi B., Volonteri M., Rossi E. M., Colpi M., Portegies Zwart S., 2012, *MNRAS*, 421, 1465  
Fan X., Bañados E. Simcoe R. A., 2023, *ARA&A*, 61, 373  
Fragione, G. Pacucci, F., 2023, *ApJL*, 958, 124  
Freitag M., Gürkan M. A., Rasio F. A., 2006, *MNRAS*, 368, 141  
Grazian A. et al., 2018, *A&A*, 613, A44  
Hirano S., et al., 2014, *ApJ*, 781, 60  
Hosokawa T., et al., 2016 *ApJ* 824 119  
Johnson J. L., Bromm V., 2007, *MNRAS*, 374, 1557  
King A. R., 2012, *MNRAS*, 421, 3443  
Kozłowski S., 2017, *ApJS*, 228, 9  
Larson, L.R., et al.,2023, . *ApJL*. 953, L29  
Latif, M. A. and Ferrara, A. 2016, *PASA*, 33, e051  
Lodato G., Natarajan P., 2006, *MNRAS*, 371, 1813  
Lupi A., Colpi M., Devecchi B., Galanti G., Volonteri M., 2014, *MNRAS*, 442, 3616  
Madau, P. & Rees, M. J, 2001,. *Astrophys. J. Lett.* 551, L27–L30,  
Maiolino, R., et al..2024, *Nature* 627, 59–63  
Mapelli, M..2016, *MNRAS*,. 459, 3432–3446  
Natrajan, P., et al., 2024 *ApJL* 960 L1  
Pacucci F. and Loeb A., 2020, *ApJ*, 895, 95  
Pacucci, F., Ferrara, A., Volonteri, M., and Dubus, G., 2015,. *MNRAS*. 454, 3771  
Planck group, 2020, *A&A*, 641, A6.  
Portegies Z., et al.,2004, *Nature* 428, 724–726  
Schneider, R., et al. 2023, *MNRAS* 526, 3250–3261  
Shang C., Bryan G. L., Haiman Z., 2010, *MNRAS*, 402, 1249  
Shen Y. et al., 2019, *ApJ*, 873, 35  
Stacy, A., Bromm, V. & Lee, A. T., 2016, *MNRAS* 462, 1307–1328.  
Volonteri, M., Habouzit, M. & Colpi, M., 2021, *Nat Rev Phys* 3, 732–743  
Xue Ge, Zhao, B-X. Bian, W-H., Frederick, G.R., 2019, *AJ*, 157, 14  
Wu, X.B., et al., 2015, *Nature*, 518, 512.  
Wyithe J. S. B., Loeb A., 2012, *MNRAS*, 425, 28  
Zubovas K. and King A., 2021,*MNRAS*, 501, 4289

## APPENDIX

Table A1 gives the data for 59 of the 91 SMBHs in Figs.1 and 2 with references for the data sources. The BHs are listed in order of their redshift  $z$  from the highest to the lowest. The first reference # is for BH's discovery paper, and the second # is for BH's mass estimate. The remaining 32 high- $z$  SMBHs are in Table 3 of Shen et al. (2019) in the order they appear.

J0002+2550; J0008-0626; J0810+5105; J0835+3217; J0836+0054; J0840+5624; J0841+2905; J0842+1218; J0850+3246; J1044-0125; J1137+3549; J1143+3808; J1148+5251; J1207+0630; J1243+2529; J1250+3130; J1257+6349; J1403+0902; J1425+3254; J1427+3312; J1436+5007; J1545+6028; J1602+4228; 1609+3041; J1621+5155; J1623+3112; J1630+4012; P000+26; P060+24; P210+27; P228+21; and P333+26

BH #	Black Hole Name	BH Mass MBH ( $M_{\odot}$ ) ( $\pm 1\sigma$ )	$z$	Age (Myr)	Ref.
1	J0313-1806	$1.6 \times 10^9$ (+0.4/-0.4)	7.64	676	1
2	ULAS J1342+0928	$9.1 \times 10^8$ (+1.3/-1.4)	7.541	688	2
3	J100758.264+211529.207	$1.5 \times 10^9$ (+0.2/-0.2)	7.52	690	3
4	ULAS J1120+0641	$2.0 \times 10^9$ (+1.5/-0.7)	7.085	747	4
5	J124353.93+010038.5	$3.3 \times 10^8$ (+2.0/-2.0)	7.07	749	5
6	J0038-1527	$1.33 \times 10^9$ (+0.25/-0.25)	7.021	756	6
7	DES J025216.64-050331.8	$1.39 \times 10^9$ (+0.16/-0.16)	7	759	7
8	ULAS J2348-3054	$2.1 \times 10^9$ (+0.5/-0.5)	6.886	775	8
9	VDES J0020-3653	$1.67 \times 10^9$ (0.32/-0.32)	6.834	783	9
10	PSO J172.3556+18.7734	$2.9 \times 10^8$ (+0.7/-0.6)	6.823	784	10
11	ULAS J0109-3047	$1.5 \times 10^9$ (+0.4/-0.4)	6.745	796	8
12	HSC J1205-0000	$2.9 \times 10^9$ (+0.4/-0.4)	6.73	799	11,12
113	VDES J0244-5008	$1.15 \times 10^9$ (+0.39/-0.39)	6.724	800	9

14	PSO J338.2298	$3.7 \times 10^9$ (+1.3/-1.0)	6.658	810	13
15	ULAS J0305-3150	$1.0 \times 10^9$ (+0.1/-0.1)	6.604	819	8
16	PSO J323.1382	$1.39 \times 10^9$ (+0.32/-0.51)	6.592	821	14
17	PSO J231.6575	$3.05 \times 10^9$ (+0.44/-2.24)	6.587	820	14
18	PSO J036.5078	$3 \times 10^9$ (+0.92/-0.77)	6.527	831	13,14
19	VDES J0224-4711	$2.12 \times 10^9$ (+0.42/-0.42)	6.526	831	9
20	PSO J167.6415	$3 \times 10^8$ (+0.08/-0.12)	6.508	834	13,14
21	PSO J261+19	$6.7 \times 10^8$ (+0.21/-0.21)	6.483	839	15
22	PSO J247.2970	$5.2 \times 10^8$ (+0.22/-0.25)	6.476	840	14
23	PSO J011+09	$1.20 \times 10^9$ (+0.51/-0.51)	6.458	843	15
24	CFHQS J0210-0456	$8 \times 10^7$ (+5.5/-4.0)	6.438	846	16
25	CFHQS J2329-0301	$2.5 \times 10^9$ (+0.4/-0.4)	6.417	850	16
26	SDSS J1148+5251	$2.7 \times 10^9$ (+0.4/-0.4)	6.41	851	17,18
27	HSC J0859 +0022	$3.8 \times 10^7$ (+0.1/-0.18)	6.388	855	11,19
28	HSC J1152 +0055	$6.3 \times 10^8$ (+0.8/-1.2)	6.36	860	11,19
29	SDSS J1148+0702	$1.26 \times 10^9$ (+0.14/-0.14)	6.339	863	20
30	SDSS J1030+0524	$1.0 \times 10^9$ (+0.2/-0.2)	6.3	870	21,22
31	SDSS J0100+2802	$1.24 \times 10^{10}$ (+0.19/-0.19)	6.3	870	23
32	CFHQS J0050+3445	$2.6 \times 10^9$ (+0.50/-0.4)	6.253	879	16
33	HSC J2239 +0207	$1.1 \times 10^9$ (+3/-2)	6.245	880	19
34	VDES J0330-4025	$5.87 \times 10^9$ (+0.89/-0.89)	6.239	881	15
35	VDES J0323-4701	$5.5 \times 10^8$ (+1.26/-1.26)	6.238	881	15

36	SDSS J1623+3112	$1.5 \times 10^9$ (+0.3/-0.3)	6.211	886	21
37	SDSS J1048+4637	$3.9 \times 10^9$ (+2.1/-2.1)	6.198	889	24
38	PSO J359-06	$1.66 \times 10^9$ (+0.21/-0.21)	6.164	895	15
39	CFHQS J0221-0802	$7 \times 10^8$ (+7.5/-4.7)	6.161	896	16
40	HSC J1208-0200	$7.1 \times 10^8$ (+2.4/-5.2)	6.144	899	19
41	ULAS J1319+0950	$2.7 \times 10^9$ (+0.6/-0.6)	6.13	902	25,26
42	CFHQS J1509-1749	$3 \times 10^9$ (+0.3/-0.3)	6.121	903	16
43	PSO J239-07	$3.63 \times 10^9$ (+0.20/-0.20)	6.114	905	15
44	HSC J2216-0016	$7 \times 10^8$ (+1.4/-2.3)	6.109	906	19
45	CFHQS J2100-1715	$3.37 \times 10^9$ (+0.64/-0.64)	6.087	910	16
46	SDSS J0303-0019	$3 \times 10^8$ (+2.0/-2.0)	6.079	911	24
47	SDSS J0353+0104	$1.4 \times 10^9$ (+1.0/-1.0)	6.072	913	24
48	SDSS J0842+1218	$1.7 \times 10^9$ (+1.2/-1.2)	6.069	913	24
49	SDSS J1630+4012	$9 \times 10^8$ (+0.8/-0.8)	6.058	915	24
50	PSO J158-14	$2.15 \times 10^9$ (+0.25/-0.25)	6.057	916	15
51	CFHQS J1641+3755	$2.4 \times 10^8$ (+1.0/-0.8)	6.047	918	16
52	SDSS J1306+0356	$1.1 \times 10^9$ (+0.1/-0.1)	6.017	923	21
53	SDSS J2310+1855	$2.8 \times 10^9$ (+0.6/-0.6)	6.003	926	27, 19
54	CFHQS J0055+0146	$2.4 \times 10^8$ (+0.9/-0.7)	5.983	930	16
55	PSO J056-16	$7.5 \times 10^8$ (+0.07/-0.07)	5.975	932	15
56	SDSS J1411+1217	$1.1 \times 10^9$ (+0.1/-0.1)	5.93	941	28, 22



57	SDSS J0005-0006	$3 \times 10^8$ (+0.1/-0.1)	5.85	957	28,22
58	SDSS J0836+0054	$2.7 \times 10^9$ (+0.6/-0.6)	5.82	964	28, 22
59	SDSS J1044-0125	$1.05 \times 10^{10}$ (+0.16/-0.16)	5.784	971	29, 21

**Table A1:: Parameters of SMBHs at  $z > 5.7$**   
**Notes: BHs are listed in order of their redshift from the highest**

**to the lowest. The first reference # is for the BH discovery paper, and the second # is for the BH mass estimate.**

### References in Table A1

- [1] Wang, F., et al., ApJL. 907, L1 (2021)
- [2] Bañados, E. et al. Nature, 553, 473 (2017).
- [3] Yang, J., et al. ApJL. 897, L14 (2020)
- [4] Mortlock, D.J., et al. Nature, 474, 616 (2011).
- [5] Matsuoka, Y., et al. ApJL 872, L2 (2019).
- [6] Wang F., et al. ApJL 869, L9 (2018).
- [7] Wang, F., et al. ApJ. 896, 23 (2020).
- [8] Venemans, B.P., et al. ApJ. 779, 24 (2013).
- [9] Reed, S.L., et al. MNRAS. 2, 1874-1885 (2019)
- [10] Bañados, E. et al. ApJ. 909, 80 (2021).
- [11] Matsuoka, Y., et al. ApJ. 828, 26 (2016).
- [12] Kato, N., et al. ASJ. 72, (5), 84 (2020).
- [13] Venemans B.P., et al. ApJL 801, L11 (2015).
- [14] Mazzucchelli, C., et al. ApJ. 849, 91 (2017)
- [15] Eilers, A.C., et al. ApJ. 900, 37 (2020)
- [16] Willott, C.J., et al. ApJ. 140, 546 (2010).
- [17] Willott, C.J., McLure, R.J., Jarvis, M.J. ApJL 587, L15 (2003).
- [18] Gallerani S. et al. MNRAS. 467, 3590.(2017).
- [19] Onoue, M., et al. ApJ. 880, 77 (2019).
- [20] Jiang, L., et al. ApJ. 833, 222 (2016).
- [21] Jiang, L., et al. ApJ. 134, 1150 (2007)
- [22] Kurk, J.D., et al. ApJ. 669, 32 (2007).
- [23] Wu, X.B., et al. Nature, 518, 512 (2015)
- [24] De Rosa, G., et al. ApJ. 739, 56 (2011)
- [25] Mortlock, D.J., et al, A&A, 505, 97 (2009)
- [26] Y. Shao, Y., et al. ApJ. 845, 138 (2017)
- [27] Wang, F., et al. ApJL. 739, L34 (2011)
- [28] Fan, X., et al. ApJ. 131, 1203 (2006)
- [29] Fan, X., et al. ApJ. 120, 1167 (2000)

